Report of the activities on Wire Development and Wire Characterization at UNIGE

Tommaso BAGNI[1], Gianmarco BOVONE[1], Florin BUTA[1], Francesco LONARDO[1], Carmine SENATORE[1,2]
[1]*Department of Quantum Matter Physics, University of Geneva, Geneva, Switzerland*
[2]*Department of Particle and Nuclear Physics, University of Geneva, Geneva, Switzerland*

Amalia BALLARINO, Bernardo BORDINI, Thierry BOUTBOUL, Jose FERRADAS, Simon C. HOPKINS
CERN, Geneva, Switzerland

After the latest update of the European Strategy for Particle Physics, released in June 2020, and with the goal of increasing the potential to discover new particles and phenomena by pushing at the energy frontier, plans are going ahead to conceive a future proton-proton collider with a center-of-mass energy of at least 100 TeV, i.e. more than 7 times the design energy of the Large Hadron Collider (LHC). A first analysis of the general parameters of this 100 TeV Future Circular Collider (FCC) leads to a baseline configuration requiring dipole magnets of 16 T in a 100 km-long tunnel. Hence, FCC requires field levels that are almost the double of the 8.3 T achieved by the Nb-Ti magnets installed in the LHC, Nb_3Sn being in the present days the preferred solution for achieving the 16 T target. From a first analysis of the main magnet design parameters, a 16 T field in a dipole configuration translates into a requirement of a minimum non-Cu J_c of more than 1'500 A/mm^2 in the superconductor at 16 T and 4.2 K (non-Cu J_c corresponds to the critical current divided by the wire cross-section area minus the Cu area). A special grade Nb_3Sn wire was industrialized for the high luminosity upgrade of LHC (HL-LHC), with values of the non-Cu J_c of about 1'000 A/mm^2 at 4.2 K, 16 T. These values are three times higher than those of the Nb_3Sn wires developed for the International Thermonuclear Experimental Reactor (ITER), but are still ~40% below the performance requirement for the 16 T dipoles of the FCC. Moreover, the superior superconducting properties of Nb_3Sn with respect to the LHC Nb-Ti conductor are impaired by its mechanical fragility, which poses critical challenges to the magnet mechanics. As a result of the large fields and current densities, the superconducting coils of an accelerator magnet experience large electromagnetic forces. In the present days, the majority of the proposed designs for the FCC dipoles entail peak stresses in the coils that are in the range of 150 – 200 MPa during magnet assembly and operation. These peak stresses are compressive and act in the transverse direction of the Nb_3Sn Rutherford cables used to wind the coils. As the local stresses approach and, in some cases, exceed the currently understood limits of the conductor, it becomes crucial to establish precisely the mechanical limits to be adopted in any of the magnet assembly, cooling and operation phases, as well as to develop methods for enhancing the mechanical limits of the conductor itself.

It was in this frame that UNIGE and CERN signed two research agreements under the auspices of CHART-2, with the goals of

1) Achieving the projected target of 1'500 A/mm^2 at 4.2 K, 16 T in a Nb_3Sn wire with proven scalability to long-length industrial production;
2) Establishing the mechanical limits at which state-of-the-art and R&D Nb_3Sn superconductors can operate safely, to enable the development of magnets whose performance is close to the inherent limitation of the conductor.

1. Wire Development: Advanced Niobium-Tin superconductors for next generation particle colliders

To achieve the highest performance possible with Nb_3Sn technology and, thus, meet the non-Cu J_c requirement for the FCC 16 T dipoles, research needs to cover a range of areas, including condensed matter physics, material engineering and applied science. The current-carrying capacity of type-II superconductors in a magnetic field is determined by their ability to prevent the movement of vortices, which is known as pinning. This is accomplished by the presence of features in the material called pinning centers, which attract individual vortices. In Nb_3Sn, grain boundaries are the main pinning centers, therefore, materials with finer grains have higher current densities. In modern high-performance wires, Nb_3Sn typically has grain sizes of 100-150 nm. The best ways to inhibit grain growth and, thus, increase the critical current performance of these wires is through the use of oxide nanoparticles, particularly through the use of the "internal oxidation" method. This method utilizes a precursor of Nb-alloys that contain a small amount of Zr or Hf, and a metal oxide powder that acts as an oxygen source. During the heat treatment, the metal oxide powder is reduced and oxygen diffuses into the Nb-alloy, oxidizing the highly reactive Zr or Hf and forming very fine particles of ZrO_2 or HfO_2 that inhibit the growth of Nb_3Sn during the reaction with Sn. For this method to be effective, the Gibbs free energy of formation of the metal oxide must be higher than that of ZrO_2 or HfO_2.

In our wire development program, we are focusing primarily on implementing the internal oxidation method in internal Sn rod-type Nb_3Sn wires, as they are closest to meeting the performance target set for the FCC. The program was divided into three phases: (i) studying the materials in monofilamentary wires, including testing different Nb-alloy compositions and oxygen sources and their combinations, (ii) developing multifilamentary wires with a reduced number of filaments and an internal Sn source, referred to as "test-bed sub-elements," and (iii) producing internally oxidized multi-filamentary wires of the internal Sn type that match the critical current performance of FCC using a process that can be scaled up for industrial production.

1.1 Internal oxidation in monofilamentary wires

Our monofilamentary wires have an external Sn configuration, in which a Nb-alloy filament 0.22 mm in diameter is surrounded by successive electrodeposited layers of Cu, Sn and Cu. In the center of the Nb-alloy, a compacted core of metal oxide powder serves as the oxygen source for the internal oxidation. Multiple combinations of different Nb-alloys and oxygen sources were studied, in an attempt to further improve the high magnetic field properties and identify materials that may be of interest for the development of the multifilamentary wires. In particular, custom Nb-alloys containing Zr and Ta were produced and tested to combine the increase in the critical current density because of the reduced grain growth to high upper critical fields because of the presence of Ta, which is a well-known dopant for increasing B_{c2}. The main properties of selected wires are summarized in Table I.

Table I. Main parameters and properties of the monofilametary wires

Filament material (wt%)	Metal oxide powder	Average grain size, short axis (nm)	Average grain size, long axis (nm)	T_c (99%) (K)	B_{c2} @ 4.2K (99% R_n) (T)
Nb-7.5Ta (ref.)	-	92	118	18.2±0.1	27.9
Nb-1Zr	SnO_2	57	95	17.7±0.1	26.7±0.1
Nb-1Zr	CuO	51	90	17.8	27.0±0.1
Nb-7.5Ta-1Zr	SnO_2	60	87	18.0±0.2	28.7±0.2
Nb-7.5Ta-2Zr	SnO_2	55	95	18.1	29.2±0.2

The data in Table I show that the grain size of Nb_3Sn in materials made with internally oxidized Nb-Zr alloys is smaller than in reference samples made with Nb-7.5Ta without added oxygen, with the smallest average grain size being around 50 nm. The grains are slightly elongated, with an aspect ratio of 1.5-1.7, and the refinement is more pronounced in the short axis direction. As a result of this refinement, the critical current densities as determined from inductive measurements up to 7 T are higher, with extrapolated layer J_c (i.e. the critical current divided by the area of the superconducting layer) at 16 T and 4.2 K of the samples containing internally oxidized Zr exceeding 3'000 A/mm^2, which is significantly above the 2'000 A/mm^2 measured in the best RRP® wires.

This work has produced also a new and important finding with technological implications: we have conclusively demonstrated that Nb_3Sn based on the Nb-7.5Ta-1Zr and Nb-7.5Ta-2Zr alloys have much higher upper critical fields than those based on Nb-7.5Ta, an alloy that otherwise was optimized as a filament material leading to a high upper critical field. The B_{c2} values measured on these samples were the highest ever recorded at 4.2 K for doped Nb_3Sn, with a value of 29.2 T at 4.2 K for the wire prepared with the Nb-7.5Ta-2Zr alloy. The upper critical fields were determined from resistive measurements at fields of up to 33 T at the European High Magnetic Field Laboratory in Grenoble, France.

1.2 Internal oxidation in test-bed sub-elements

The next step in the development of multi-filamentary wires of the internal Sn type using internally oxidized Nb-alloys was the production of test-bed sub-elements with a reduced number of filaments. Internal Sn rod-type wires are made restacking a large number of sub-elements. Each sub-element contains typically of more than one hundred Nb-alloy filaments inside a Cu matrix with a Sn core at the center. Our test-bed sub-elements consist of twelve Nb-alloy filaments in a Cu matrix around a Sn core, with the filaments made from the alloys Nb-1Zr, Nb-7.5Ta-1Zr, and Nb-7.5Ta-2Hf (all weight percentages). This design allowed us to efficiently and quickly test a variety of alloy and oxygen source configurations in a versatile and flexible internal Sn architecture.

Two methods were tested for introducing the oxygen source (SnO_2 or CuO nano-sized powders) and were evaluated based on their effects on the superconducting properties and the assembly's deformability:

1) Core Oxide: This approach is similar to the one used for mono-filamentary wires. A hole is drilled in the center of the Nb-alloy rod, filled with oxide nano-powders, and then the rod is deformed to the desired dimensions for the assembly of the sub-element;
2) Annular Oxide: The oxide powder is introduced between the Nb-alloy and Cu. The oxide is deposited through a dip-coating process on the surface of the Nb-alloy rod, which is then inserted into a Cu tube.

Both methods result in the diffusion of oxygen from the powder source into the Zr- or Hf-containing Nb-alloys during the heat treatment, leading to the formation of ZrO_2 or HfO_2 nanoparticles and the subsequent refinement of the Nb_3Sn grains. Figure 1 shows the cross section of the test-bed sub-elements, reacted following a two-plateau schedule with 100 h at 550°C followed by 200 h at 650°C, and high magnification views of their Nb_3Sn microstructure. The images allow us to make a direct comparison of the grain size of Nb_3Sn in wires without oxygen source in the composite, with SnO_2 in the core of the filaments, and with SnO_2 in the annular configuration, all made with the same starting Nb-alloys. The introduction of SnO_2 in both core and annular approach permits to reduce the grain size of Nb_3Sn from ~100 nm in the reference wires without oxygen to approximately 50 nm. The internally oxidized samples also have a reduced thickness of the Nb_3Sn layer, indicating a slower diffusion of Sn in the Nb-alloy. The thickness decreased from 20-25 µm in the test-bed sub-elements without an

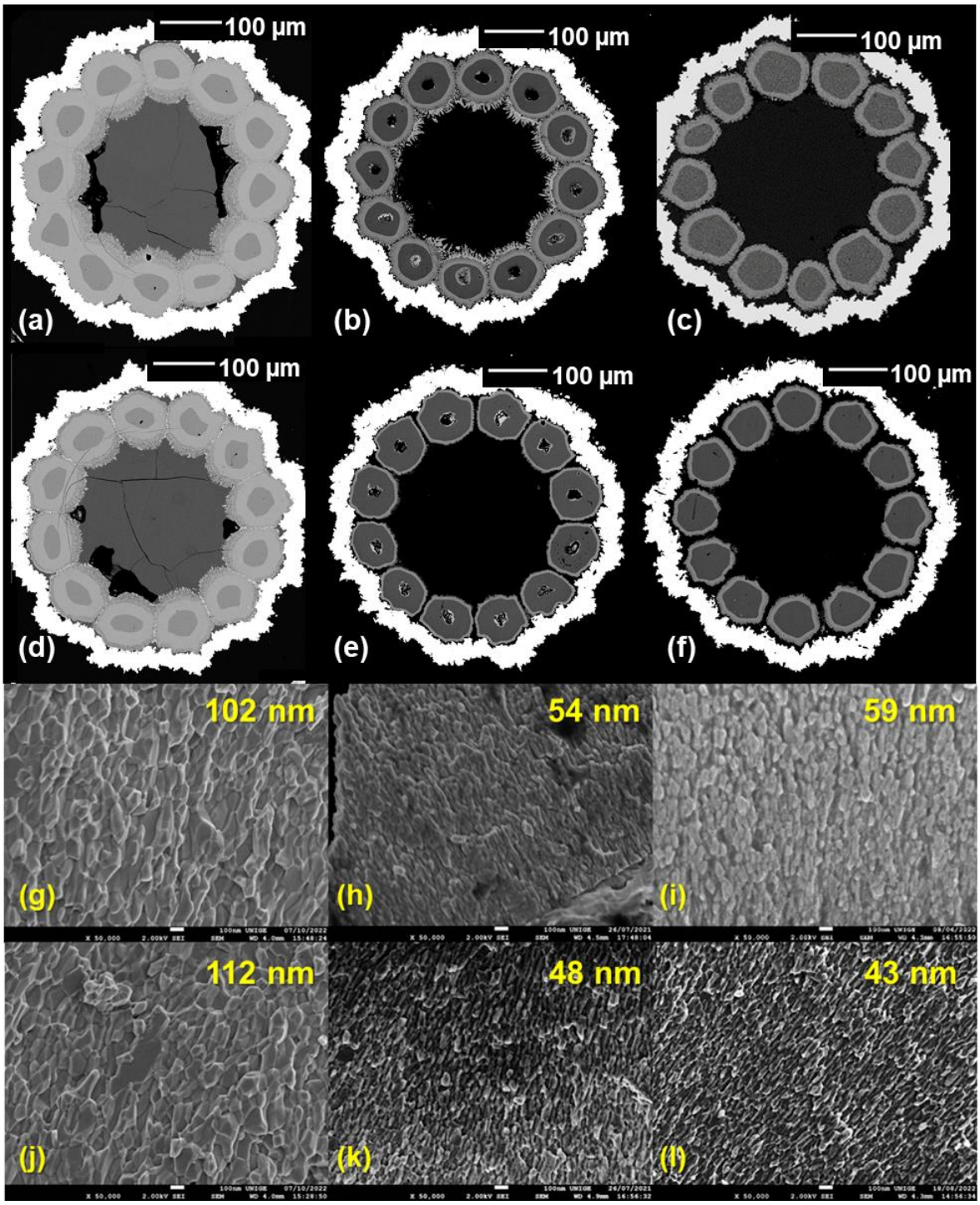

Figure 1 SEM images of the test-bed sub-element cross sections (a)-(f) and of the corresponding Nb_3Sn grains at fractured surfaces (g)-(l) for samples based on Nb-7.5Ta-1Zr in (a) and (g), Nb-7.5Ta-1Zr + SnO_2 in the core configuration in (b) and (h), Nb-7.5Ta-1Zr + SnO_2 in the annular configuration in (c) and (i), Nb-7.5Ta-2Hf in (d) and (j), Nb-7.5Ta-2Hf + SnO_2 in the core configuration in (e) and (k), and Nb-7.5Ta-2Hf + SnO_2 in the annular configuration in (f) and (l), respectively. The refinement of the grain size in the samples containing an oxygen source is evident.

oxygen source to 4-8 µm in those with an internal oxygen source, regardless of its configuration. We are currently conducting studies to optimize the heat treatment and promote the growth of the Nb_3Sn layer of internally oxidized samples by adjusting temperature and duration of the second plateau. Increasing the temperature or duration can lead to a thicker reaction layer, but it also causes grain coarsening, which negatively affects the critical current performance. The optimization study is still

ongoing; however, our current findings indicate that samples treated at 700°C for 100 hours produce Nb_3Sn layers as thick as 15 µm while still maintaining grain sizes below 60 nm.

Transport critical current measurements have been performed on selected samples at 4.2 K and in magnetic fields up to 19 T. Samples with oxidation have a significantly higher layer-J_c compared to those without oxidation, as illustrated in Figure 2. The internally oxidized samples made with Zr alloy have a layer-J_c of 2'600-2'700 A/mm^2 at 4.2 K and 16 T, while those made with Hf alloy have a slightly higher value at 3'000 A/mm^2. Considering that the non-Cu J_c of a high-performance

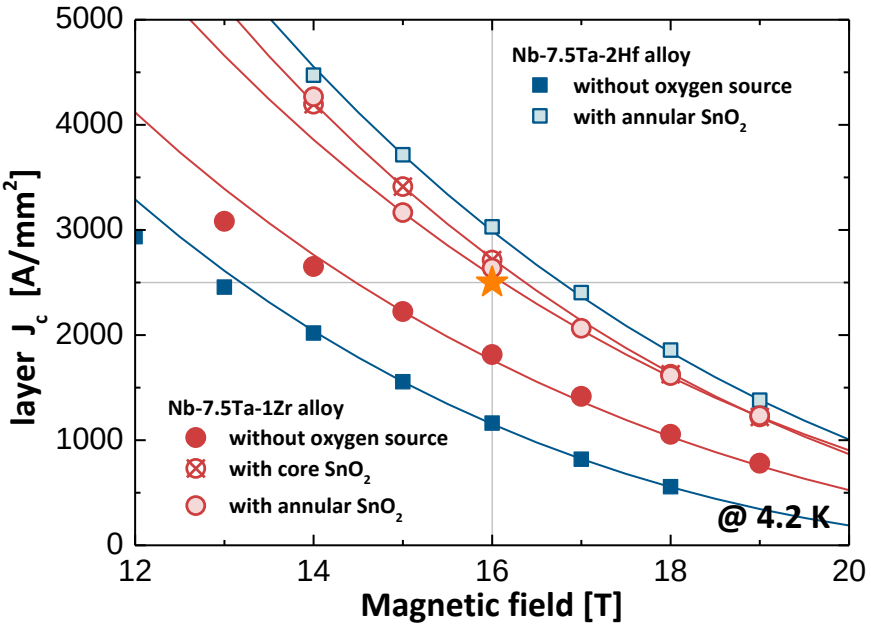

Figure 2 Layer J_c at 4.2 K extracted from transport critical current measurements for test-bed sub-elements based on Nb-7.5Ta-1Zr without oxygen source (solid circles), Nb-7.5Ta-1Zr with SnO_2 in the core configuration (crossed circles), Nb-7.5Ta-1Zr with SnO_2 in the annular configuration (open circles), Nb-7.5Ta-2Hf without oxygen source (solid squares) and Nb-7.5Ta-2Hf with SnO_2 in the annular configuration (open squares). All samples were heat treated at 550°C/100h + 650°C/200h. The enhancement of the layer J_c at values exceeding the FCC target at 16 T is recorded for all the samples with internal oxidation.

commercial Nb_3Sn wire is about 60% of its layer-J_c, these results indicate that the performance of these test-bed sub-elements exceeds the FCC target, which translates into a layer-J_c of 2'500 A/mm^2 at 4.2 K and 16 T.

Additionally, we conducted measurements on the electrical resistance of over 50 samples in temperatures ranging from 2.5 to 14 K and magnetic fields up to 35 T to determine the temperature dependence of B_{c2}. These measurements were performed at the European High Magnetic Field Laboratory in Grenoble. We evaluated B_{c2} for test-bed sub-elements made with different architectures and starting materials, testing multiple samples of each type. Our results showed that adding an oxygen source improves B_{c2} in both Hf and Zr doped samples. Using SnO_2 in annular configuration, we found an average B_{c2} value at 4.2 K of 29.2 T and 29.3 T for Zr- and Hf-added samples respectively, with a maximum value of 29.5 T for one of the Hf-added samples. These values support our previous findings on monofilamentary wires. Further investigation is being conducted to understand the exact role of oxide precipitates in increasing B_{c2} through X-Ray Adsorption Spectroscopy studies at PSI and Transmission Electron Microscopy observation.

A summary including the main properties of selected test-bed sub-elements is reported in Table II.

Table II. Main parameters and properties of selected test-bed sub-elements heat treated at 550°C/100h + 650°C/200h

Filament material (wt%)	Metal oxide powder	Metal oxide configuration	Average grain size, (nm)	B_{c2} @ 4.2K (99% R_n) (T)
Nb-7.5Ta-2Hf	-	-	112	28.9±0.5
Nb-7.5Ta-2Hf	SnO_2	Core	48	29.0±0.3
Nb-7.5Ta-2Hf	SnO_2	Annular	43	29.3±0.2
Nb-7.5Ta-1Zr	-	-	102	28.0±0.6
Nb-7.5Ta-1Zr	SnO_2	Core	54	29.0±0.4
Nb-7.5Ta-1Zr	SnO_2	Annular	59	29.2±0.2

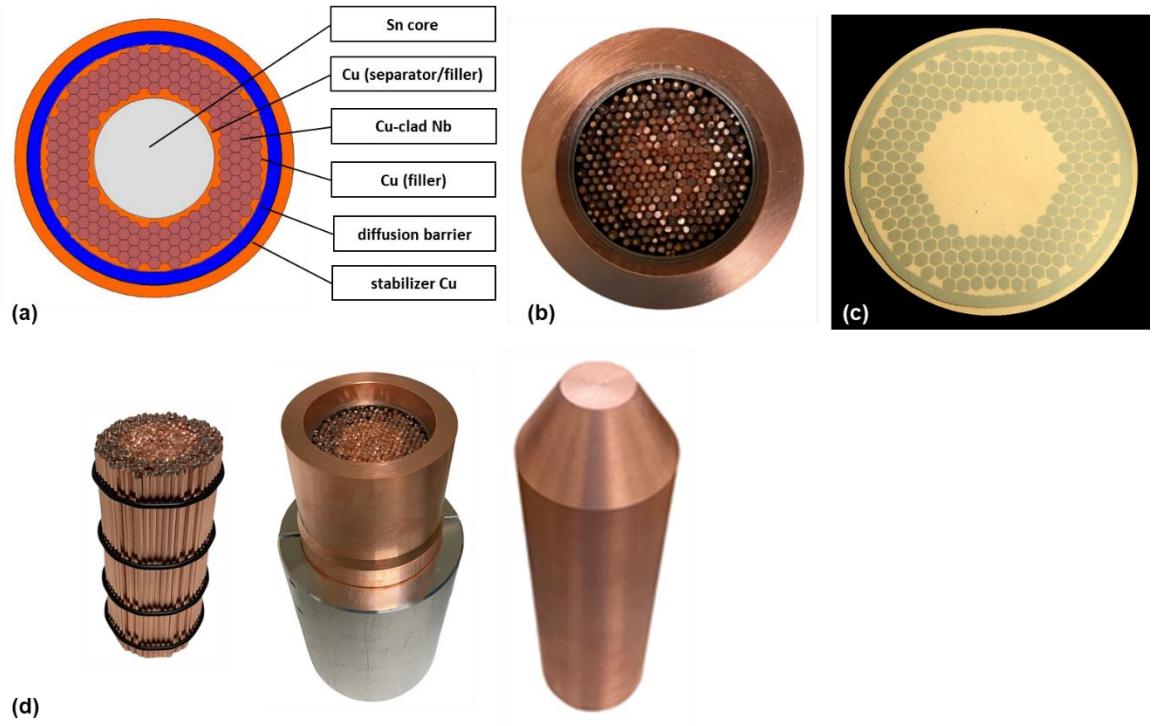

Figure 3 (a) Sub-element configuration used for the first series of prototype wires; (b) sub-element assembly for the extrusion billet with an outer diameter of 75 mm; (c) polished cross-section of the extruded rod at 19.8 mm prior to be gun drilled for Sn insertion; (d) different stages of the billet preparation.

1.3 Prototype Internal Sn wires

It was already mentioned in the previous section that internal Sn rod-type Nb_3Sn wires, also referred to as Restacked-Rod-Process (RRP®) wires, are composed of a repetitive unit known as a sub-element, which has a distinct design. In this design, the Sn is positioned in the center of an extruded rod that contains Nb-alloy filaments, a diffusion barrier, and a Cu matrix. The wire is then produced stacking and cold drawing several sub-elements in a high purity Cu tube (typically oxygen-free electronic Cu, OFE-Cu) down to the wire final size.

Based on the positive results obtained at the test-bed sub-element scale, we are advancing now with the development of the first series of prototype wires. It was decided that this first series, which includes a reference wire and others with internal oxidation, will have the same sub-element configuration: a number of 192 Cu/Nb-alloy hexagonal filament rods placed around 121 sacrificial filament rods made of Cu and surrounded by a Nb sheet barrier (the diffusion barrier in the finale wire) in an OFE-Cu cylinder as represented in Figure 3. Some of the 192 Cu/Nb-alloy hexagonal filament rods

may nevertheless be replaced with a similarly sized oxygen carrying filament rods. This 192/121 configuration was chosen because it can accommodate the proper Nb/Sn ratio when the Nb content in the Cu/Nb filament rods is pushed to the high values of 80-90% that can lead to high non-Cu critical current densities.

Using the basic configuration described above we have machined and assembled a billet using Nb-7.5Ta filaments. Round Cu/Nb-Ta rods prepared by swaging and drawing deformation were hexagonally shaped to 2.46 mm between parallel faces and then stacked with 121 Cu filaments in a billet with a outer diameter of 75 mm, according to the configuration of Figure 3. After compaction by

HIP the billet was hydrostatically extruded to a round rod of 19.8 mm diameter. The extruded rod for this reference wire was gun drilled and is currently being prepared for Sn insertion and further deformation. After drawing to a diameter somewhere between 1 and 1.5 mm the resulted wire will be hexagonally shaped and restacked/co-drawn with hexagonal Cu wires in a Cu tube to form the final internal Sn wire. The resulted wire will serve as reference in comparing the processing and the properties with those of wire of the same design but based on Nb-7.5Ta-1Zr and Nb-7.5Ta-2Hf alloys with oxygen sources. A second billet has been assembled based on the Nb-7.5Ta-2Hf alloy where some of the Cu/Nb-alloy filaments were replaced with tubes filled with a metal oxide. We are currently getting ready for the HIP compaction of this new billet in view of its hydrostatic extrusion.

Financial support to this activity is also provided by the Swiss National Science Foundation (Grant No. 200021_184940).

2. Wire Characterization: Multiphysical properties of advanced superconductors

Accelerator magnet's coils are wound using insulated Rutherford cables composed of many single wires transposed together. These cables are ultimately resin-impregnated, conforming a solid winding pack intended for a homogeneous distribution of the mechanical loads inside the coils. In dipoles, the azimuthal component of the electromagnetic forces during operation accumulates at the midplane of the coil, with a magnitude of many hundreds kN/m. In the same way, the radial component pushes the coil outwards with a maximum displacement localized again at the midplane, while the axial component tends to elongate the coil. The mechanical design of the magnets aims to avoid deformation or movement of the conductor during powering, which may lead to premature quenches, and this is achieved by applying a mechanical pre-compression to the superconducting coils when assembling the magnet. However, the combination of pre-compression, thermal stresses during heat treatment and during the cooldown at cryogenic temperature, and electromagnetic forces arising in the operation regime exposes the brittle and strain sensitive Nb_3Sn to the risk of irreversible reduction of its critical current performance. Restricting ourselves to the operation regime, the most severe loads are the ones acting in the transverse direction of the Rutherford cables and usually located in the coils' mid-planes. In a scenario where the design of next generation accelerator magnets entails peak stresses in the coils that are in the level of 150 – 200 MPa, the degradation of the conductor performance due to mechanical strain appears to be a parameter of the highest importance for Nb_3Sn-based accelerator magnets. Hence, several laboratories have developed dedicated experiments aimed at testing the mechanical sensitivity of Nb_3Sn, in which a conductor – a full Rutherford cable, a sub-scale cable or a single wire – is exposed to mechanical loads relevant to accelerator magnet applications.

At the University of Geneva, we developed an experiment with the scope to extract from tests on single wires quantitative information about the degradation of a Rutherford cable under transverse

stress. We perform measurements of the critical current, I_c, on single Nb_3Sn wires submitted to transverse compressive loads at 4.2 K. Wires are resin-impregnated to imitate the working conditions in the Rutherford cables of accelerator magnets. During our experiments, samples are exposed to load/unload cycles at low temperature under increasing transverse stress values and this allows us to determine the reversible and irreversible components of the measured reduction of I_c. Three types of Nb_3Sn wire have been so far investigated in the frame of the CHART-2 collaboration. Two of them are Restacked-Rod-Process (RRP®) wires composed of 108 sub-elements embedded in a high-purity Cu matrix following the 108/127 hexagonal restack, with a nominal copper to non-copper ratio (Cu/non-Cu) equal to 1.2. They differ in diameter: the wire at 0.7 mm belongs to one of the production billets developed for the 11 T dipoles of HL-LHC, while that at 0.85 mm was extracted from a billet produced for use in the new interaction regions quadrupoles of HL-LHC, identified by the acronym MQXF. The third wire is a Powder-In-Tube (PIT) wire with 192 filaments and a Cu/non-Cu volume ratio of approximately 1.22. It has a diameter of 1.0 mm and was produced for the FRESCA2 dipole project at CERN. Both round and 15%-rolled wire samples have been investigated as a part of the measurement campaign. The rolled samples seek to mimic the deformation of the superconducting wires due to cabling. In particular, the 15%-rolling, i.e. a height reduction corresponding to 15% of the wire diameter, is used to qualify the wires for the HL-LHC project in terms of the effects on the electrical properties produced by cabling.

In the following, the irreversible stress limit, σ_{irr}, of a wire is defined as the stress value leading to a reduction of I_c after unload by 5% with respect to the critical current at zero applied stress, I_{c0}. This is a convention and the value of σ_{irr} is typically extracted from the measurements performed with an external magnetic field B = 19 T. The degradation of the critical current performance after unload and, more generally, the electro-mechanical response of impregnated Nb_3Sn wires to transverse stress are determined by a combination of different factors, which are intrinsic and extrinsic to the wires. They include: (i) the wire technology and its filament layout, (ii) the way mechanical loads are applied to the wire and the wire's geometry (round or 15% rolled) and (iii) the stiffness of the resin system used for impregnation.

2.1 Influence of the wire technology on the irreversible stress limit

Our experiments revealed marked differences in terms of tolerance to transverse stress between the measured RRP® and PIT wires, which follow directly from the different wire technologies. Figure 4 compares the evolution of the critical current under load and after unload for the three wires described above. The wires were impregnated with a mixture of epoxy type L and filler and tested at B = 19 T. We measured σ_{irr} = 155 MPa for the RRP® wire at 0.70 mm, 175 MPa for the RRP® wire at 0.85 mm and 110 MPa for the PIT wire at 1.0 mm. There is a clear indication of a higher tolerance to transverse stress of RRP® wires compared to the PIT one, which is related to the differences in the internal architecture of the wire composites. In particular, the mechanical properties of the materials left at the center of the Nb_3Sn sub-elements or filaments after reaction are very different for RRP® and PIT wires and are expected to play a role in the electromechanical properties: the core of an RRP® sub-element consists of a solid low-Sn bronze matrix embedding a large number of micrometric voids, while the reacted filaments of PIT wires contain a poorly connected powder core where the reaction remainders are aggregated. On the other hand, the difference in the σ_{irr} values of the two RRP® wires could be considered *a priori* an unexpected result, as the layout of their sub-elements is identical. The reduction of the transverse stress tolerance observed in the 0.70 mm-wire may be influenced by the heat treatment schedule. Following the recipe used at CERN, the final step of the heat treatment for the 0.70 mm-wire was performed at 650°C for 50 hours, i.e. at a lower temperature compared to the 665°C used for the reaction of the 0.85 mm-wire keeping the same duration. The lower temperature

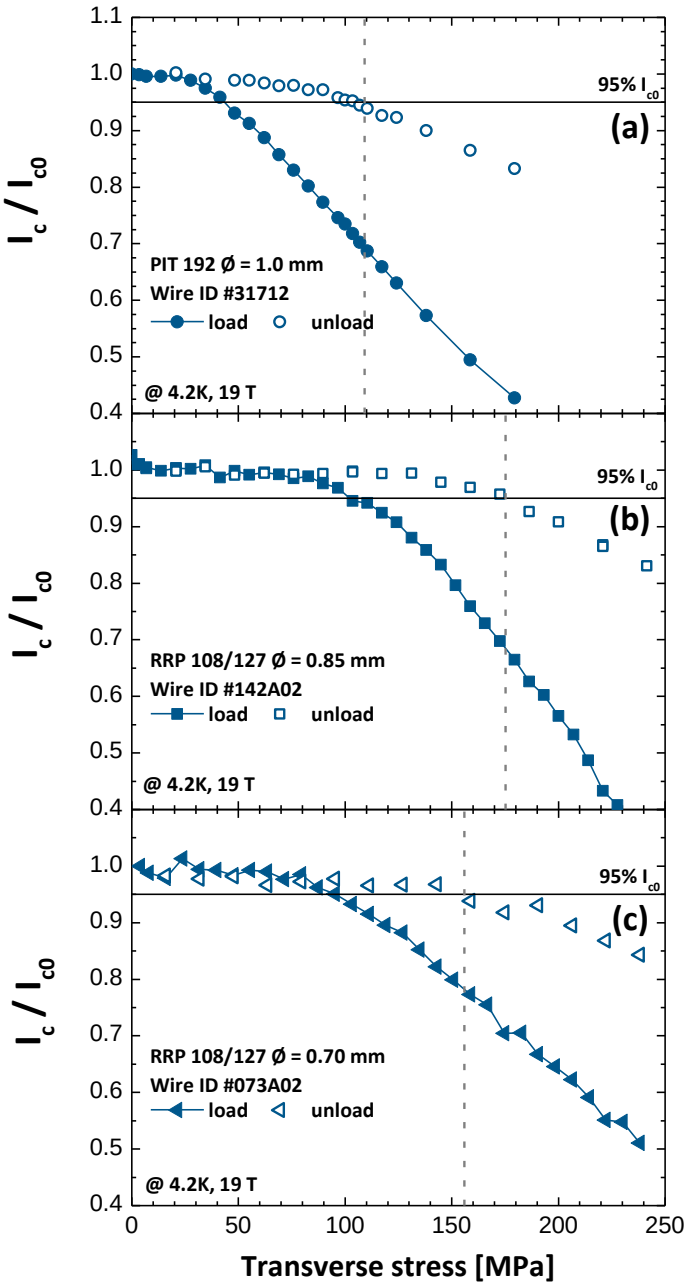

Figure 4 Dependence on the applied transverse stress at T = 4.2 K, B = 19 T of the critical current I_c normalized to the critical current at zero applied stress, I_{c0}, for (a) the 1-mm PIT wire, measured in a 1.15-mm wide groove; (b) the 0.85-mm RRP wire, measured in a 1.15-mm wide groove; (c) the 0.70-mm RRP wire, measured in a 1.0-mm wide groove. All wires were impregnated with epoxy type L. Solid and open symbols correspond to the measurement under load and after unload, respectively. Dashed lines indicate the conventionally defined irreversible stress limits.

allows preserving a high residual resistivity ratio, RRR, of the Cu-matrix also in the smaller wire diameter, which is needed to ensure the stability of magnets against quenching. Nonetheless, a reduction of the electromechanical limits when decreasing the heat-treatment temperature was documented in the literature and confirmed in various wire designs of RRP® wires.

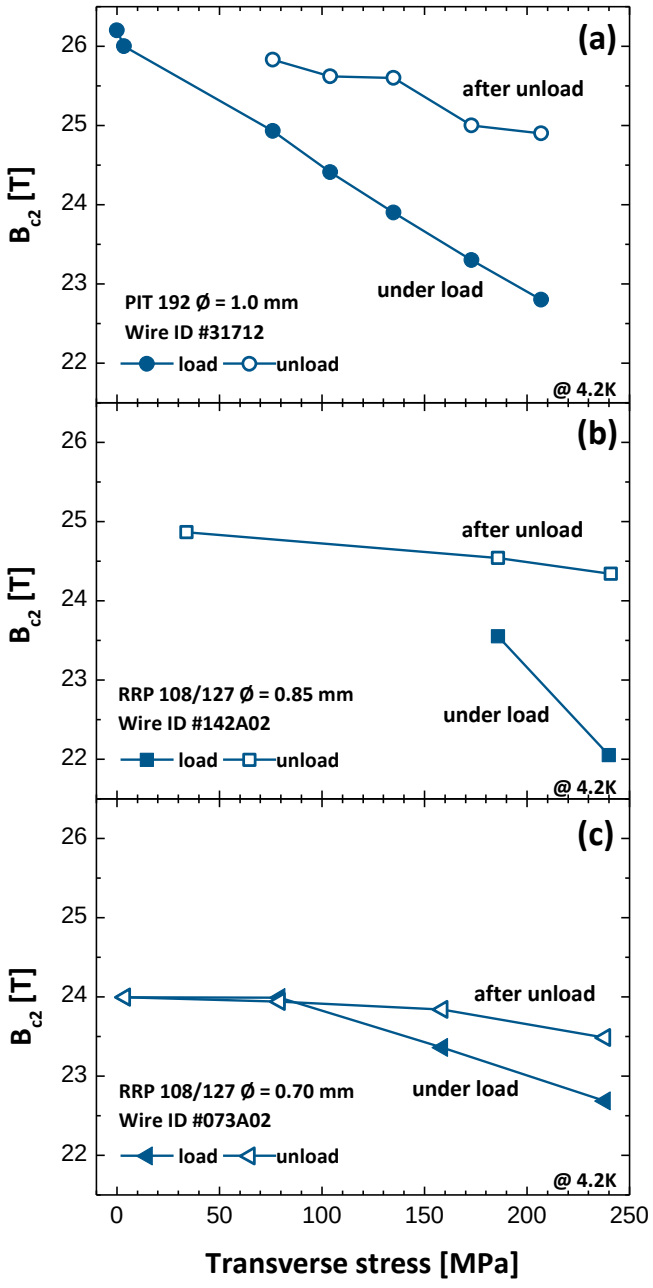

Figure 5 Upper critical field, B_{c2}, under load (solid symbols) and after unload (open symbols) as a function of the applied transverse stress for (a) the 1-mm PIT wire, measured in a 1.15-mm wide groove; (b) the 0.85-mm RRP wire, measured in a 1.15-mm wide groove; (c) the 0.70-mm RRP wire, measured in a 1.0-mm wide groove. The observed decrease of B_{c2} after unload from increasing stress values witnesses the presence of the residual stresses acting on Nb_3Sn.

The permanent reduction of the critical current observed when the load is removed occurs for two reasons, which can be concomitant: (1) the residual stress imposed to Nb_3Sn by the plastically-deformed Cu matrix and (2) the formation of cracks in the Nb_3Sn layer. Even if both mechanisms can lead to the irreversible reduction of the critical current after unload, I_c^{unload}, their effects are expected to be different. Similarly to what is observed when the wire is under load, the distortion of the Nb_3Sn lattice due to residual stress determines a reduction of the upper critical field after unload, B_{c2}^{unload}, with respect to the value measured on the virgin wire, $B_{c2,0}$. On the other hand, when cracks are present in the Nb_3Sn layer, even if the critical current density of the superconductor is in principle preserved, the total current-carrying cross-section and, thus, I_c^{unload} can be reduced.

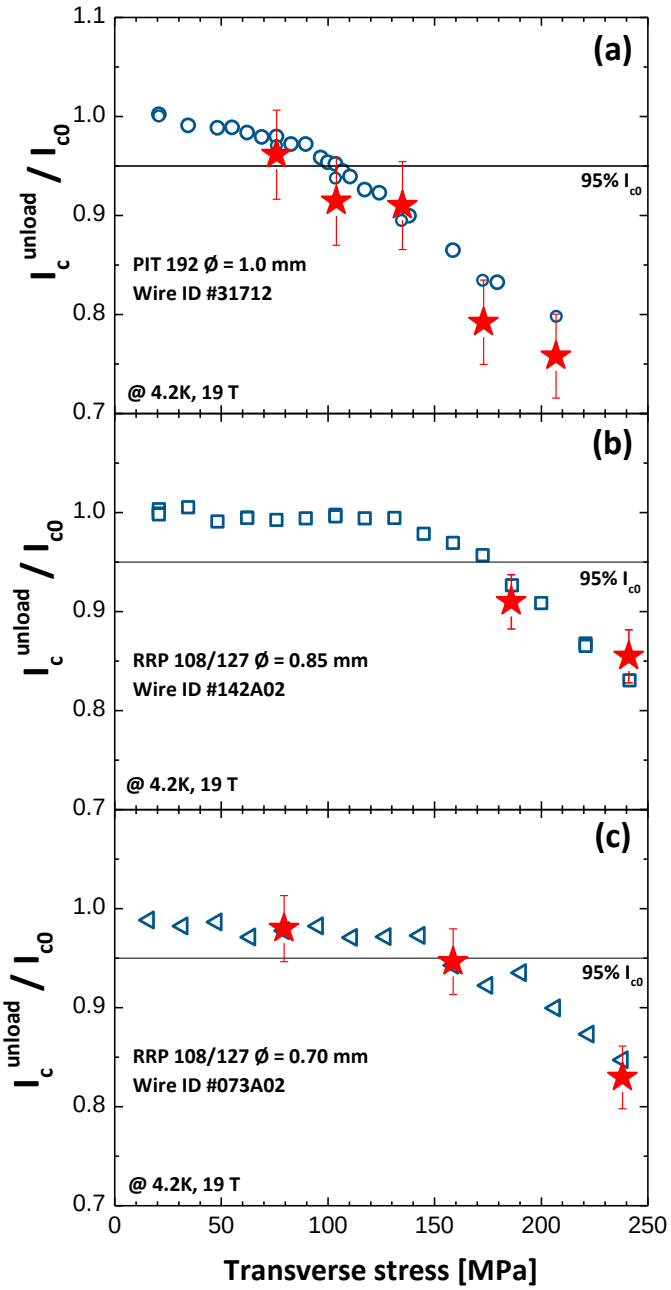

Figure 6 Evolution of the normalized critical current after unload, I_c^{unload}/I_{c0}, as a function of the applied transverse stress for (a) the 1-mm PIT wire, measured in a 1.15-mm wide groove; (b) the 0.85-mm RRP wire, measured in a 1.15-mm wide groove; (c) the 0.70-mm RRP wire, measured in a 1.0-mm wide groove. The solid stars represent the expected values of I_c^{unload}/I_{c0} as predicted using our model.

We developed a method to identify the dominant degradation mechanism from the evolution of the upper critical field after stress unload, B_{c2}^{unload}, along the transverse loading history. Moreover, this method allows us predicting the fraction of critical current lost after unload due to the residual stresses imposed to Nb_3Sn by the plastically deformed Cu matrix. In Figure 5 the stress dependence of the upper critical field under load, B_{c2}^{load}, and after unload, B_{c2}^{unload} for the three type of wires examined in the frame of the project is shown. Each point of B_{c2}^{unload} is represented at the value of σ from which the unload started. The most important result of Figure 5 is the continuous decrease of B_{c2}^{unload} after unload from increasing stress values. A reduction of more than 1 T with respect to $B_{c2,0}$ is measured after the last unload from 210 MPa in the PIT wire, while the final unload from 240 MPa leads to a drop

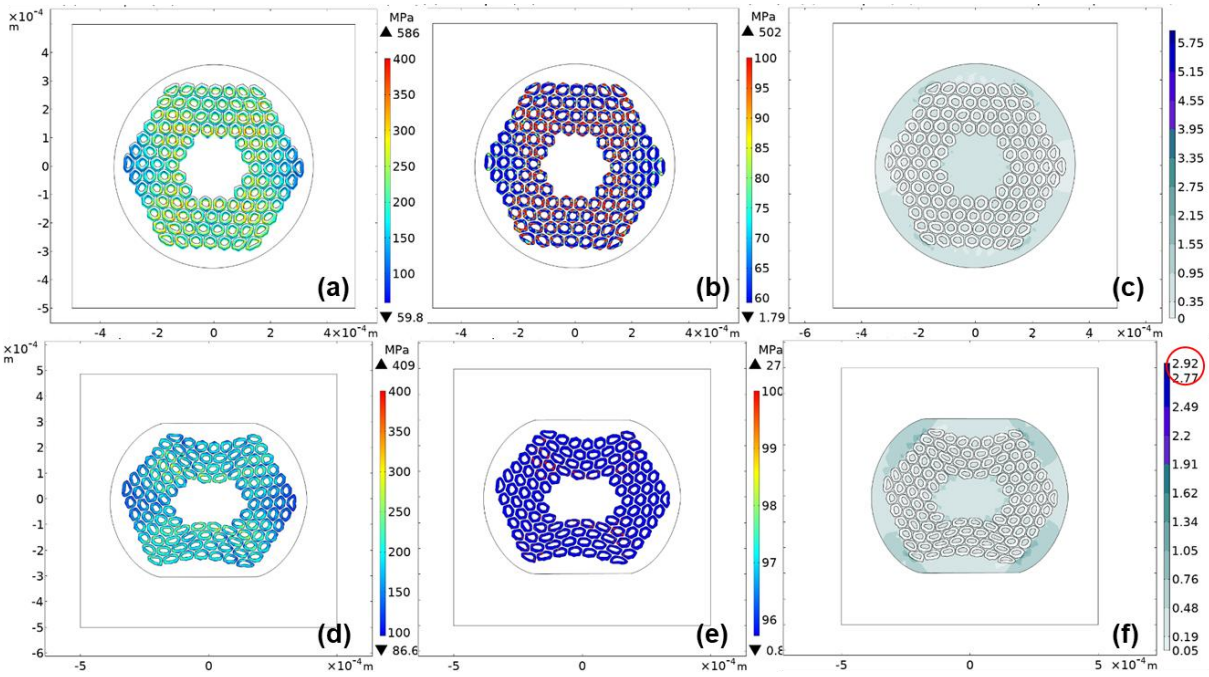

Figure 7 FEM simulations of the Von Mises stress distribution in Nb_3Sn when a transverse force of 30 kN is applied (a) to a 108/127 RRP® round wire and (d) to the same wire with 15%-rolling deformation. FEM simulations of the residual Von Mises stress in Nb_3Sn after unload from 30 kN for (b) the round wire and for (e) the 15%-rolled wire. FEM simulations of the plastic strain in copper after unload from 30 kN for (c) the round wire and for (f) the 15%-rolled wire.

of about 0.5 T for the two RRP wires. These experiments provide a clear indicator of the residual stresses acting on Nb_3Sn. However, this result is not sufficient by itself to rule out the presence of cracks as concomitant cause of the reduction of I_c^{unload}. Figure 6 shows the normalized critical current after unload measured at 19 T together with the expected permanent reduction of I_c due to residual stresses, as calculated using our model. Very interestingly, the measured reduction of I_c^{unload} from stress values as high as 240 MPa can be fully accounted for with the reduction of B_{c2}^{unload} due to residual stress, regardless of the type of wire. Cracks and breakages in Nb_3Sn seem to have a negligible effect on the permanent degradation of the critical current in the geometry of our experiment, i.e. for an impregnated wire confined in a groove and submitted to transverse compressive load. Similar conclusions were drawn at CERN from the analysis of the critical current reduction under transverse stress of Rutherford cables based on the same type of PIT Nb_3Sn wires tested at UNIGE.

2.2 *Influence of the wire geometry on the irreversible stress limit*

Further evidences of the dominant role of residual stresses in the degradation of I_c^{unload} emerged from the tests performed on the 15%-rolled wires. In these experiments, the transverse force was applied to the flat surface of the rolled wires. An increase of σ_{irr} was anticipated because the mechanical load applied to the flattened wire is expected to lead to a more favorable stress redistribution in the composite compared to situation of the round wire. This hypothesis was confirmed by the result of the experiments performed on the RRP® wires, whose diameter before rolling was 0.70 mm. Differently from the PIT wires, RRP® wires do not experience a reduction in I_c as a result of the rolling process. Moreover, the irreversible stress limit for the rolled wires is higher by about 30 MPa compared to that of the round wires, the value of σ_{irr} measured at B = 19 T being 185 MPa and 155 MPa, respectively.

In the frame of a collaboration with Dr. Ciro Calzolaio from PSI, a mechanical Finite Element Model (FEM) was created to analyze the redistribution of the stress within the wire composite when applying the transverse load to a round wire and to a 15%-rolled wire. The model was based on a 2D plain strain

approach and accounts for the elastoplastic properties of the materials. The wire geometries were extracted from scanning electron microscope (SEM) images of the real RRP® wire cross sections, using an analysis algorithm based on machine learning, and then imported in COMSOL. The main outcomes of the simulations are summarized in Figure 7: the images in the top row correspond to the results obtained for the round wire, while those in the bottom row were computed for the 15%-rolled wire. The panels (a) and (d) of Figure 7 show the Von Mises stress distribution in Nb_3Sn when a transverse force of 30 kN is applied. The residual Von Mises stress in Nb_3Sn after unload from 30 kN is computed in the panels (b) and (e). Finally, the plastic strain in copper after unload from 30 kN is reported in the panels (c) and (f). It is evident from the comparison of the simulations for the round wire and the 15%-rolled one that the transverse load applied to the rolled wire produces, for a given value of the external force, less plastic strain in the copper matrix and thus lower values of the residual Von Mises stress in Nb_3Sn after unload. Further studies are ongoing, but the measured increase of σ_{irr} in the rolled wires find a straightforward interpretation based on the simulation results.

2.3 *Influence of the impregnation stiffness on the irreversible stress limit*

The stiffness of the impregnation is an extrinsic factor with a large impact on the irreversible stress limit. We have performed a comparative study by testing:

- A bare PIT wire impregnated with a mixture of epoxy type L and a filler; the elastic modulus of this loaded epoxy is comparable to the one of CDT-101K, which is the resin used for the impregnation of large coils for accelerator magnets.
- A bare PIT wire impregnated with Stycast, whose elastic modulus is about double compared to CDT-101K and epoxy type L.
- A PIT wire inserted in a glass-fiber sleeve and impregnated with the regular mixture of epoxy type L and filler.

The conclusion of the study was that adding rigidity to the impregnation moves the onset of the irreversible reduction of the wire critical current toward higher stresses. In our tests, we measured an increase of σ_{irr} of about 50 MPa by replacing the epoxy type L with Stycast or by adding a glass-fiber reinforcement to the wire impregnated with epoxy type L.

2.4 Analysis of the crack formation in Nb_3Sn wires by deep learning applied to X-ray tomography

As a complement to the electro-mechanical tests, we have also developed a novel non-destructive and non-invasive method to investigate crack formation and propagation in high-performance Nb_3Sn wires by combining X-ray tomography images, which were taken at the High Energy Scattering beam line of the European Synchrotron Radiation Facility (ESRF), and deep learning networks.

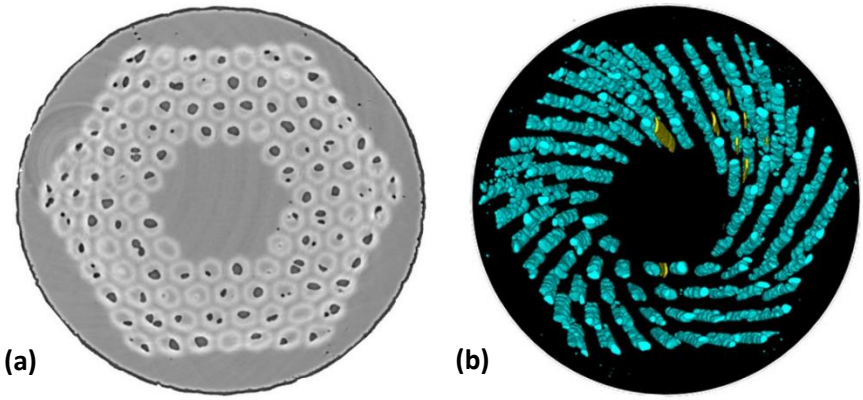

Figure 8 Tomographic cross section of the 0.70-mm RRP wire after the final unload from 240 MPa, as measured at ESRF. (b) 3D reconstruction by Convolutional Neural Networks of the voids and cracks in the wire volume. Voids are displayed in cyan while cracks in yellow.

In a first step, our analysis tool was based on an unsupervised machine learning algorithm able to autonomously isolate, reconstruct and analyze the voids in the superconducting filament structure, which are formed mostly during the activation heat treatment and determine localized stress concentration and possibly the formation of cracks. This culminated in the development of the tomography analysis tool (TAT), a python-based free software for image analysis based on k-means. By implementing deep learning Convolutional Neural Networks in the analysis, the tool became able to identify also the cracks formed inside the Nb_3Sn filaments. In particular, tomography images were taken on the RRP® wire sample at 0.7 mm extracted from the I_c vs transverse stress probe at the end of the experiment after the final unload from 240 MPa. Figure 8(a) shows a tomography cross section of the wire. Figure 8(b) provides a 3D perspective of the voids in cyan and of the cracks in yellow, as detected by deep learning. The wire volume examined by tomography corresponds to a scan length of about 1.5 mm. Only very few cracks are present in the examined sample after unload from 240 MPa. These cracks are up to 30 μm-long in the transverse direction with a maximum width of ~5 μm, while they propagate beyond the scan length of 1.5 mm in the longitudinal direction. However, none of the observed cracks creates interruptions in the sub-elements, which could lead to a reduction of the active cross-section. This observation supports the conclusion that the irreversible reduction under transverse compression of the critical current is only marginally influenced in our experiment by the presence of cracks.

3. Publications

[1] T. Bagni, D. Mauro, M. Majkut, A. Rack, C. Senatore, "Formation and propagation of cracks in RRP Nb_3Sn wires studied by deep learning applied to x-ray tomography," Supercond. Sci. Technol., vol. 35, 104003, 2022
https://doi.org/10.1088/1361-6668/ac86ac

[2] T. Bagni, H. Haldi, D. Mauro, C. Senatore, "Tomography analysis tool: an application for image analysis based on unsupervised machine learning," IOPSciNotes, vol. 3, 015201, 2022
https://doi.org/10.1088/2633-1357/ac54bf

[3] F. Buta, M. Bonura, D. Matera, G. Bovone, A. Ballarino, S. C. Hopkins, B. Bordini, X. Chaud, C. Senatore, "Nb_3Sn superconductors with internally oxidized Zr and Ta doping: Superconducting properties and microstructure," J. Phys. Mater, vol. 4, 02503, 2021.
https://doi.org/10.1088/2515-7639/abe662

[4] T. Bagni, G. Bovone, A. Rack, D. Mauro, C. Barth, D. Matera, F. Buta, C. Senatore, "Voids in RRP Nb_3Sn wire and their implications on electro-mechanical and electrothermal stability: an X-ray tomography analysis," Sci. Reports, vol. 11, 7767, 2021

https://doi.org/10.1038/s41598-021-87475-6
[5] J. Ferradas Troitino, T. Bagni, C. Barth, B. Bordini, P. Ferracin, L. Gamperle, D. Tommasini, D. Zurmuehle, C. Senatore, "Effects of the initial axial strain state on the response to transverse stress of high-performance RRP Nb_3Sn wires," Supercond. Sci. Technol., vol. 34, 035008, 2021
https://doi.org/10.1088/1361-6668/abd388
[6] L. Gämperle, J. Ferradas, C. Barth, B. Bordini, D. Tommasini, C. Senatore, "Determination of the electromechanical limits of high-performance Nb_3Sn Rutherford cables under transverse stress from a single-wire experiment," Phys. Rev. Research., vol. 2, p. 013211, 2020.
https://doi.org/10.1103/PhysRevResearch.2.013211

4. Presentations at conferences and workshops

- *The influence of the oxygen-source layout on the high-field behavior of internally-oxidized multifilamentary Nb_3Sn wires*
  Presenting author: Gianmarco BOVONE, contributed oral at ASC2022, the Applied Superconductivity Conference, Honolulu, USA, October 23 – 28, 2022;
- *Degradation of I_c in high-performance Nb_3Sn wires: a study combining electromechanical investigations and machine learning applied to X-Ray tomography*
  Presenting author: Carmine SENATORE, contributed oral at ASC2022, the Applied Superconductivity Conference, Honolulu, USA, October 23 – 28, 2022;
- *Frontiers of Nb_3Sn conductor technology for applications in high field accelerator magnets*
  Presenting author: Carmine SENATORE, invited oral at IEEE CSC Italy Chapter Workshop, Rome, Italy, June 13, 2022;
- *Recent developments of Nb_3Sn wires for application*
  Presenting author: Carmine SENATORE, invited oral at ISS2021, the 34nd International Symposium on Superconductivity, virtual event, November 30 – December 2, 2021;
- *Deep learning applied to X-ray tomography as a new tool to analyze the formation and propagation of cracks in RRP Nb_3Sn wires*
  Presenting author: Tommaso BAGNI, contributed oral at EUCAS2021, the 15th European Conference on Applied Superconductivity, virtual event, September 5 – 9, 2021;
- *Evaluation of approaches to introduce oxygen sources for the internal oxidation of Zr and Hf in rod type Nb_3Sn wires*
  Presenting author: Gianmarco BOVONE, invited oral at EUCAS2021, the 15th European Conference on Applied Superconductivity, virtual event, September 5 – 9, 2021;
- *Degradation of I_c after mechanical unload in high performance Nb_3Sn wires: the role of filament breakages and residual stress*
  Presenting author: Carmine SENATORE, contributed oral at EUCAS2021, the 15th European Conference on Applied Superconductivity, September 5 – 9, 2021;
- *Frontiers of Nb_3Sn and REBCO Conductor Technology for Future Applications in High Magnetic Fields*
  Presenting author: Carmine SENATORE, invited oral at MRS Spring Meeting 2021, virtual event, April 17 – 23, 2021;
- *X-ray tomography analysis of voids' distribution and morphology in high-performance RRP Nb_3Sn wires for the next generation accelerator magnets*
  Presenting author: Tommaso BAGNI, contributed oral at ASC2020, the Applied Superconductivity Conference, virtual event, October 24 – November 7, 2020;
- *Superconducting properties and oxygen diffusion in Ta-doped Nb_3Sn wires with internally oxidized ZrO_2*
  Presenting author: Florin BUTA, contributed oral at ASC2020, the Applied Superconductivity Conference, virtual event, October 24 – November 7, 2020;

- *Effects of the initial axial strain state on the response to transverse stress of high-performance RRP Nb_3Sn wires*
  Presenting author: Jose FERRADAS TROITINO, contributed oral at ASC2020, the Applied Superconductivity Conference, virtual event, October 24 – November 7, 2020;
- *Improvement of J_c and further enhancement of B_{c2} in Ta-doped Nb_3Sn with internally oxidized ZrO_2 particles*
  Presenting author: Carmine SENATORE, invited oral at SuperFOx 2020, the 5th Conference on Superconductivity and Functional Oxides, Santa Margherita Ligure, Italy, February 10 – 12, 2020.